Environmental Science & Technology

pubs.acs.org/est

Article

Separating Daily 1 km $PM_{2.5}$ Inorganic Chemical Composition in China since 2000 via Deep Learning Integrating Ground, Satellite, and Model Data

Jing Wei,* Zhanqing Li,* Xi Chen,* Chi Li, Yele Sun, Jun Wang, Alexei Lyapustin, Guy Pierre Brasseur, Mengjiao Jiang, Lin Sun, Tao Wang, Chang Hoon Jung, Bing Qiu, Cuilan Fang, Xuhui Liu, Jinrui Hao, Yan Wang, Ming Zhan, Xiaohong Song, and Yuewei Liu

Cite This: https://doi.org/10.1021/acs.est.3c00272

Read Online

ACCESS | Metrics & More | Article Recommendations | Supporting Information

ABSTRACT: Fine particulate matter ($PM_{2.5}$) chemical composition has strong and diverse impacts on the planetary environment, climate, and health. These effects are still not well understood due to limited surface observations and uncertainties in chemical model simulations. We developed a four-dimensional spatiotemporal deep forest (4D-STDF) model to estimate daily $PM_{2.5}$ chemical composition at a spatial resolution of 1 km in China since 2000 by integrating measurements of $PM_{2.5}$ species from a high-density observation network, satellite $PM_{2.5}$ retrievals, atmospheric reanalyses, and model simulations. Cross-validation results illustrate the reliability of sulfate (SO_4^{2-}), nitrate (NO_3^-), ammonium (NH_4^+), and chloride (Cl^-) estimates, with high coefficients of determination (CV-R^2) with ground-based observations of 0.74, 0.75, 0.71, and 0.66, and average root-mean-square errors (RMSE) of 6.0, 6.6, 4.3, and 2.3 $\mu g/m^3$, respectively. The three components of secondary inorganic aerosols (SIAs) account for 21% (SO_4^{2-}), 20% (NO_3^-), and 14% (NH_4^+) of the total $PM_{2.5}$ mass in eastern China; we observed significant reductions in the mass of inorganic components by 40−43% between 2013 and 2020, slowing down since 2018. Comparatively, the ratio of SIA to $PM_{2.5}$ increased by 7% across eastern China except in Beijing and nearby areas, accelerating in recent years. SO_4^{2-} has been the dominant SIA component in eastern China, although it was surpassed by NO_3^- in some areas, e.g., Beijing−Tianjin−Hebei region since 2016. SIA, accounting for nearly half (~46%) of the $PM_{2.5}$ mass, drove the explosive formation of winter haze episodes in the North China Plain. A sharp decline in SIA concentrations and an increase in SIA-to-$PM_{2.5}$ ratios during the COVID-19 lockdown were also revealed, reflecting the enhanced atmospheric oxidation capacity and formation of secondary particles.

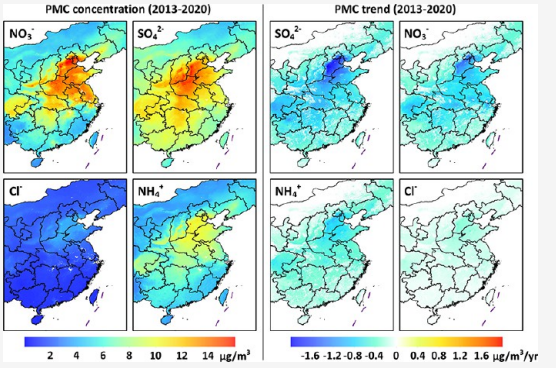

KEYWORDS: *$PM_{2.5}$ composition, secondary inorganic aerosols, deep learning, remote sensing, China*

1. INTRODUCTION

Fine particulate matter with diameters less than 2.5 μm ($PM_{2.5}$) poses a major environmental health risk around the world, especially in low- and middle-income countries.[1,2] Its chemical composition includes organic matter, black carbon, sulfate (SO_4^{2-}), nitrate (NO_3^-), ammonium (NH_4^+), chloride (Cl^-), mineral dust, and trace elements, among others. These components can be categorized into primary and secondary aerosols. The former refers to fine particles directly emitted from different pollution sources, and the latter refers to new particles formed from gaseous or particulate pollutants through photochemical and heterogeneous reactions. Secondary inorganic aerosols (SIA = SO_4^{2-} + NO_3^- + NH_4^+) are closely associated with anthropogenic emissions from the energy, industrial, and agricultural sectors.[2−4] Cl^- is an important component of sea-salt aerosols, while anthropogenic sources include coal/biomass combustion and industrial processes, influencing aerosol particle growth, atmospheric chemical reactions, $PM_{2.5}$ and ozone air quality, especially in developing countries.[5−9] For effective policy-making, monitoring changes in these inorganic components can better reflect changes in specific aerosol sources relative to the total $PM_{2.5}$.[10,11]

$PM_{2.5}$ composition has noticeable impacts on the ecological environment, ambient air quality, and Earth's climate. Acid rain formed by sulfuric and nitric acid particles via the oxidation of sulfur dioxide (SO_2) and nitrogen oxides (NO_x) affects plant growth.[12,13] The formation of SIA components is a main cause

Special Issue: Data Science for Advancing Environmental Science, Engineering, and Technology

Received: January 10, 2023
Revised: April 17, 2023
Accepted: April 17, 2023
Published: April 28, 2023

of severe haze pollution.[14,15] Sulfate aerosols with moderately long life cycles can cause significant local pollution and even affect global climate change through atmospheric transport and climate response.[16] Different $PM_{2.5}$ constituents impact human health in different ways.[17,18] Recent studies have suggested that carbonaceous aerosols from agricultural residue biomass burning and wildfires,[19,20] ultrafine particles from automobile exhaust,[21,22] and severe haze episodes caused by fine particles[23,24] have strong toxicities. Despite the general recognition of the strong health impacts of $PM_{2.5}$, the possible effects of chemical composition on these health hazards are less clear, largely due to the lack of adequate monitoring in diverse environments.

China is an emerging country with rapid industrialization and economic development in recent decades, where $PM_{2.5}$ pollution (especially SIAs) has always been a major concern in urban air quality.[25] Many studies have investigated the sources and impacts of $PM_{2.5}$ composition. However, most of these studies have involved only a few individual observation stations or specific observation periods in megacities or urban agglomerations.[26−30] Such studies likely have limitations in spatial representation because they mostly reflect the atmospheric composition around a ground site or during short-term periods. Insights from atmospheric chemistry models, e.g., Modern-Era Retrospective Analysis for Research and Applications, Version 2 (MERRA-2), Goddard Earth Observing System (GEOS)-Chem, and Weather Research and Forecasting-Community Multiscale Air Quality (WRF-CMAQ), can provide regional-to-global perspectives of long-term variations in different $PM_{2.5}$ species but tend to be biased toward certain species given limitations in main inputs such as emission inventories.[3,31] Also, model simulations are computationally costly and generally have a coarse horizontal grid resolution of tens of kilometers, limiting their applications across urban-residential scales.

$PM_{2.5}$ has been estimated from satellite remote sensing of aerosol optical depth (AOD), but little has been done with regard to aerosol composition. The long-term evolution of global $PM_{2.5}$ components was assessed by integrating satellite $PM_{2.5}$ retrievals, GEOS-Chem-simulated $PM_{2.5}$ composition information and coincident profiles, and surface $PM_{2.5}$ and composition observations.[10,32−34] $PM_{2.5}$ composition was estimated in other regions with moderate to high resolutions incorporated with surface measurements, such as in southern California at 4.4 km using a generalized additive model,[35] in the northeastern United States at 1 km combining a chemical transport model and geographically weighted regression model[11] or a land-use regression model,[36] and in North America at different resolutions with spatially smoothing models.[37,38] However, $PM_{2.5}$ composition may have strong spatial gradients due to localized sources and short lifetimes, leading to large estimation uncertainties, especially in regions with sparse observations. This has also been the case in China, where only a handful of studies relying strongly on model simulations have been done.[39,40]

What are the concentrations of major species and their proportions to total $PM_{2.5}$ mass in China, and what are their temporal changes and impacts on air quality? To address these outstanding questions, we have generated a long-term, daily, seamless $PM_{2.5}$ chemical composition product in China at a 1-km resolution by applying artificial intelligence to a large ensemble of data sets consisting of ground-based observations of aerosol composition, satellite-derived $PM_{2.5}$ at a 1-km resolution,[25] and various auxiliary data, i.e., meteorological reanalyses, pollution emission inventories, and model simulations. Different from previous studies, a stronger deep forest model, which takes advantage of multiple tree-based machine-learning models, was adopted with extensions of multidimensional spatiotemporal heterogeneity made to construct robust nonlinear relationships between each $PM_{2.5}$ component and the total $PM_{2.5}$ mass concentration. The applicability of this unique data set is also demonstrated in the analysis of atmospheric composition and changes during heavy haze episodes and the coronavirus pandemic.

2. MATERIALS AND METHODS

2.1. Data Sources. *2.1.1. Ground-Measured $PM_{2.5}$ and Composition.* Ground-based measurements of $PM_{2.5}$ composition were collected from the Chinese Center for Disease Control and Prevention network. The network includes 126 ground monitoring stations across mainland China, providing long-term (2013 to present) and high-frequency daily measurements of major water-soluble inorganic ions of $PM_{2.5}$, including SO_4^{2-}, NO_3^-, NH_4^+, and Cl^-. Most stations of $PM_{2.5}$ speciation are located in eastern China (Figure S1). The network is relatively uniform with dense clusters located in the three major economic zones (outlined by purple delineates) centered around the major megacities in China, where emissions are strong and more localized. The urban and suburban/rural sites account for 61% and 39%, respectively. As such, their spatial representativeness is sound overall, similar to the national $PM_{2.5}$ observation network.[41] Quartz filter membranes were used to collect $PM_{2.5}$ samples, followed by ion chromatography providing chemical composition information about the samples after ultrasonic extraction with pure water. For SO_4^{2-}, NO_3^-, NH_4^+, and Cl^-, the detection limits are 0.03, 0.03, 0.02, and 0.01 $\mu g/m^3$, and the relative standard errors are 0.50−1.67%, 0.16−0.96%, 0.27−1.13%, and 0.21−0.72%, respectively.[42,43] Here, daily mean SO_4^{2-}, NO_3^-, NH_4^+, and Cl^- concentrations at each station from 2013 to 2020 were used for model training and validation. Besides, daily mean in situ total $PM_{2.5}$ concentrations, provided by the China National Environmental Monitoring Centre network, were collected. For spatial matching, ground measurements were assigned to the nearest grid matching the individual site and 1-km^2 grid, and if there were two or more sites falling in the same grid, additional averaging was done.

2.1.2. Satellite $PM_{2.5}$ and Auxiliary Data. Our latest version (V4) of the long-term (2000 to present) daily seamless data set of ground-level $PM_{2.5}$ across China, i.e., the ChinaHighPM$_{2.5}$ data set from the ChinaHighAirPollutants (CHAP) database, was used in this study. It was generated from the Moderate Resolution Imaging Spectroradiometer (MODIS) Multiangle Implementation of Atmospheric Correction (MAIAC) AOD product at a 1-km resolution,[44] together with ground-based measurements of surface $PM_{2.5}$ and ample auxiliary variables, using a space-time extra-trees model.[25] The data set is of high quality with an out-of-sample cross-validated coefficient of determination (CV-R^2) of 0.92, an average root-mean-square error (RMSE) of 10.76 $\mu g/m^3$, and a mean absolute error (MAE) of 6.32 $\mu g/m^3$, compared to surface observations. It has been widely used in studies concerning public health, the environment, and the economy;[45−49] thus, it is employed here as the primary constraint of total $PM_{2.5}$ mass for separating different chemical components. Other satellite remote-sensing products related to land surface cover, topography, and

https://doi.org/10.1021/acs.est.3c00272
Environ. Sci. Technol. XXXX, XXX, XXX−XXX

population density were also used, derived from MODIS vegetation index (1 km), Shuttle Radar Topography Mission (90 m), and LandScan (1 km) products, respectively.

2.1.3. Model and Reanalysis Data. Model data employed were hourly and every 3 h surface mass concentrations of primary aerosol diagnostics (i.e., $PM_{2.5}$ inorganic components) derived from the MERRA-2 (~0.625° × 0.5°) and GEOS-forward processing (GEOS-FP) (~0.3125° × 0.25°) models. We also used monthly precursors of aerosol particles indicating anthropogenic emissions and chemical reactions, including ammonia (NH_3), NO_x, SO_2, and volatile organic compounds (VOCs) from the Copernicus Atmosphere Monitoring Service (CAMS) monthly global emission inventories (~0.1° × 0.1°).[50] Meteorological conditions affect the formation, transport, and removal of air pollutants, as well as $PM_{2.5}$ composition through particle hygroscopic growth and chemical reaction rate. Thus, hourly meteorological data were employed as model inputs, including temperature, precipitation, evaporation, winds near the surface (10 m) and in the middle troposphere (850 hPa), and surface pressure (~0.1° × 0.1°) from the ERA5-Land reanalysis,[51] as well as boundary layer height and relative humidity (~0.25° × 0.25°) from the ERA5 climate reanalysis.[52] All hourly level meteorological and chemical composition simulations were averaged or accumulated to obtain daily values. The finer-resolution input parameters were aggregated, while the coarser-resolution ones were resampled to the 1-km resolution (≈0.01° × 0.01°) using the bilinear interpolation approach.[25] Table S1 provides detailed information on all of the data used.

2.2. Methodology. *2.2.1. $PM_{2.5}$ Composition Modeling and Validation.* Relative to $PM_{2.5}$, sources and changes in its chemical composition are more complex. To improve the $PM_{2.5}$-composition separation, adopted here is a more powerful deep-learning model with a stronger data-mining capability, i.e., deep forest.[53,54] Similar to but different from the deep neural network, it is constructed by relying on the nondifferentiable decision tree instead of the differentiable neuron, i.e., based on the forest model, stacking ensemble learning with further optimization, solving the overfitting problem occurring in the deep layer. The multi-grained scanning method is applied to generate input features via the sliding window. The deep forest framework is built in a cascade forest structure adopting two kinds of forests, i.e., random forests and completely random tree forests. Each layer of training is independent supervised learning, and the number of model layers can be adaptively determined through iterative validation. The multilayer training results are integrated using the Light Gradient Boosting Machine (LightGBM) model to determine the final output. Compared with the traditional deep learning of a neural network, it has a higher training speed and uses fewer superparameters that do not need much adjustment. Also, the complexity of the model can be automatically adjusted.

Air pollutants are spatiotemporally heterogeneous, and accounting for this in models can enhance the model capability.[55,56] Here, we extend the deep forest by optimizing the way to determine spatiotemporal information on independent variables, i.e., weighted effects referencing polar coordinates compared to previous studies,[54,56,57] leading to a new model called the four-dimensional spatiotemporal deep forest (4D-STDF) model (Figure S2). Unequal autocorrelation and difference of points in space (Ps) are expressed in Euclidean space with three spherical coordinates [$S1$, $S2$, $S3$] (eq 1). The temporal characteristics of points (Pt) are expressed by three helix-shape trigonometric vectors [$T1$, $T2$, $T3$] (eq 2) to include both seasonal cycles and daily variations of air pollution.[58]

$$Ps = [S1, S2, S3] = \left[\cos\left(2\pi\frac{Lon}{360}\right)\cos\left(2\pi\frac{Lat}{180}\right), \cos\left(2\pi\frac{Lon}{360}\right)\sin\left(2\pi\frac{Lat}{180}\right), \sin\left(2\pi\frac{Lon}{360}\right)\right] \quad (1)$$

$$Pt = [T1, T2, T3] = \left[\frac{DOY}{N}, \cos\left(2\pi\frac{DOY}{N}\right), \sin\left(2\pi\frac{DOY}{N}\right)\right] \quad (2)$$

where Lon and Lat indicate the longitude and latitude of one point in space, respectively, and DOY and N represent the day of the year and the total number of days in a year, respectively.

Ground-based measurements of $PM_{2.5}$ chemical components are true values, and satellite-retrieved $PM_{2.5}$ is taken as the main input to the 4D-STDF model, together with all auxiliary factors, including MERRA-2 and GEOS-FP simulations of $PM_{2.5}$ components, CAMS emission inventories, ERA5 meteorological fields, three surface-related and population variables, and space-time terms, for training. Here, three widely used 10-fold cross-validation approaches, i.e., out-of-sample, out-of-station, and out-of-day procedures, performed by randomly discarding 10% of the data samples (overall accuracy), monitors (spatial prediction ability), and days (temporal prediction ability), respectively, are used to generate independent training and validation samples and characterize the model performance in separating different $PM_{2.5}$ components, respectively.[17] The linear regression equation and coefficient of determination (R^2) are used to quantitatively evaluate the model accuracy, and RMSE and MAE are used to evaluate the model uncertainty.

2.2.2. Model Variable Importance. Our model is superior in physical interpretation to traditional black-box deep-learning models because it can quantitatively evaluate the contribution (importance) of each input variable in separating $PM_{2.5}$ composition. Being the sum of all species, $PM_{2.5}$ carries the bulk of changes and contributes 36−45% for the three SIA components (Figure S3), followed by meteorological conditions (importance score = 22−31%). The boundary layer height is particularly critical by affecting the vertical distribution and mixing of air pollutants. Spatiotemporal information is important for modeling, accounting for 7−11%. Emission inventory and model simulations also have large impacts of 7−10% and 3−8%, respectively. The remaining factors are less important but still contribute >1%, so they are included in our model.

3. RESULTS AND DISCUSSION

Applying the 4D-STDF model to the aforementioned input data sets, we have created a daily spatially complete (gapless) data set of $PM_{2.5}$ inorganic composition over China at a 1-km resolution from 2013 to 2020 and extended the model to reconstruct historical records dating back to 2000, called ChinaHighPMC, one of a series of ChinaHighAirPollutants (CHAP) data sets. Figure S4 shows the annual maps of four

https://doi.org/10.1021/acs.est.3c00272
Environ. Sci. Technol. XXXX, XXX, XXX−XXX

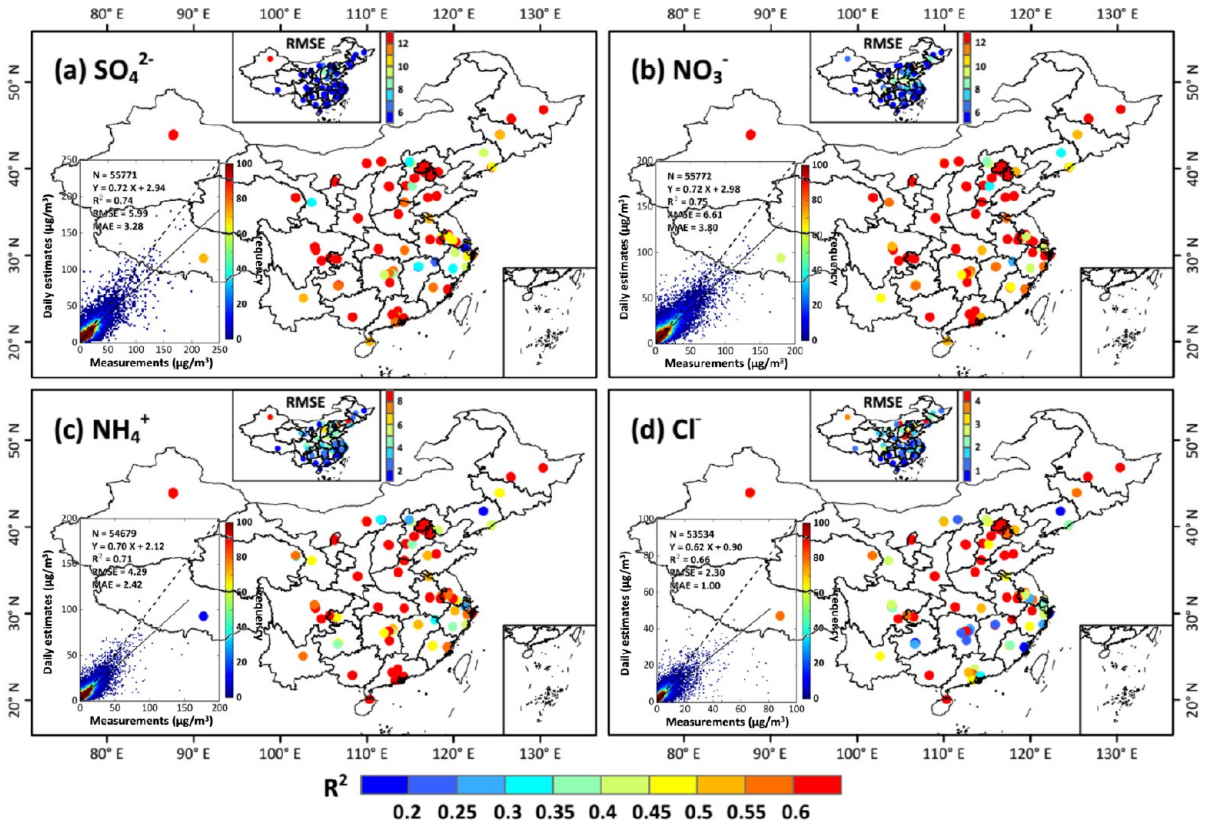

Figure 1. Overall accuracies of daily estimates ($\mu g/m^3$) of $PM_{2.5}$ inorganic components: (a) SO_4^{2-}, (b) NO_3^-, (c) NH_4^+, and (d) Cl^- at each monitoring station (maps with colored dots) and for the whole of China (inserted density scatter plots) for the period 2013−2020.

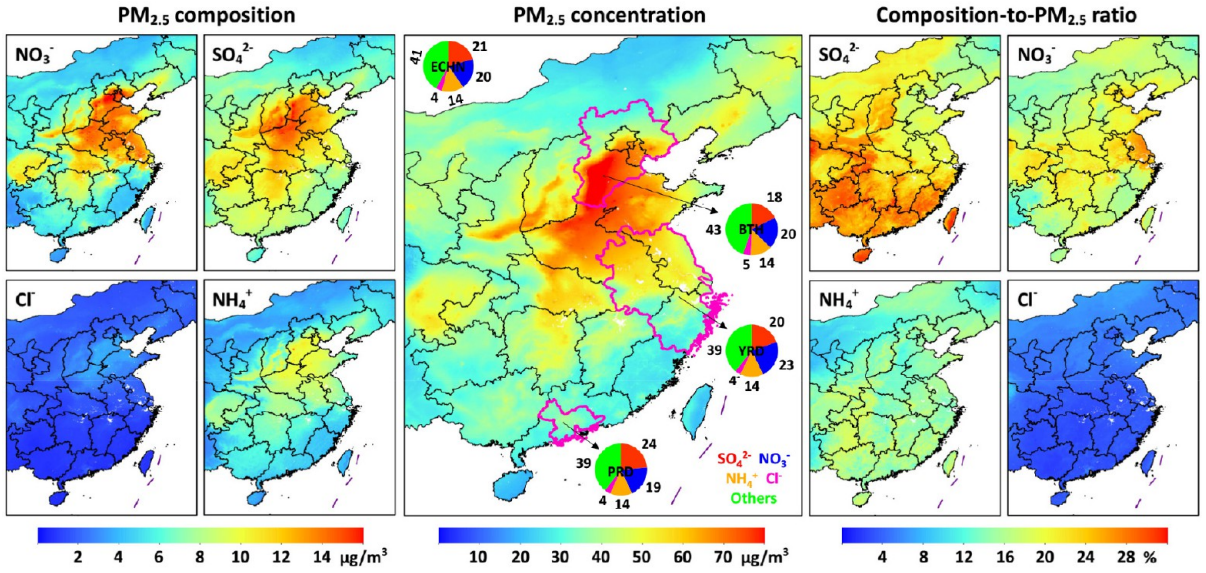

Figure 2. Spatial distributions of annual mean 1-km-resolution total $PM_{2.5}$ concentration ($\mu g/m^3$, central panel), $PM_{2.5}$ inorganic components ($\mu g/m^3$, left set of panels), and composition-to-$PM_{2.5}$ ratios (%, right set of panels) of SO_4^{2-}, NO_3^-, NH_4^+, and Cl^- in eastern China averaged over the period 2013−2020. The inserted pie charts in the middle figure show the proportions (%) of different $PM_{2.5}$ components in eastern China (ECHN) and three urban agglomerations (outlined by pink borders): the Beijing−Tianjin−Hebei (BTH) region, the Yangtze River Delta (YRD), and the Pearl River Delta (PRD).

$PM_{2.5}$ inorganic components averaged from daily data during the last two decades in eastern China.

3.1. Evaluation of Separated $PM_{2.5}$ Components. In total, ∼220,000 data samples were acquired for the four inorganic components from 2013 to 2020 at all available sites in China. Our model can differentiate $PM_{2.5}$ into different species at varying spatial scales. Sample-based cross-validations against ground measurements show a moderate correlation coefficient (CV-R^2 > 0.4) at approximately 89%, 95%, 88%, and 80% of the stations for SO_4^{2-}, NO_3^-, NH_4^+, and Cl^-, respectively (Figure 1). A few stations in northwest and central China had large estimation uncertainties. In general, the

https://doi.org/10.1021/acs.est.3c00272
Environ. Sci. Technol. XXXX, XXX, XXX−XXX

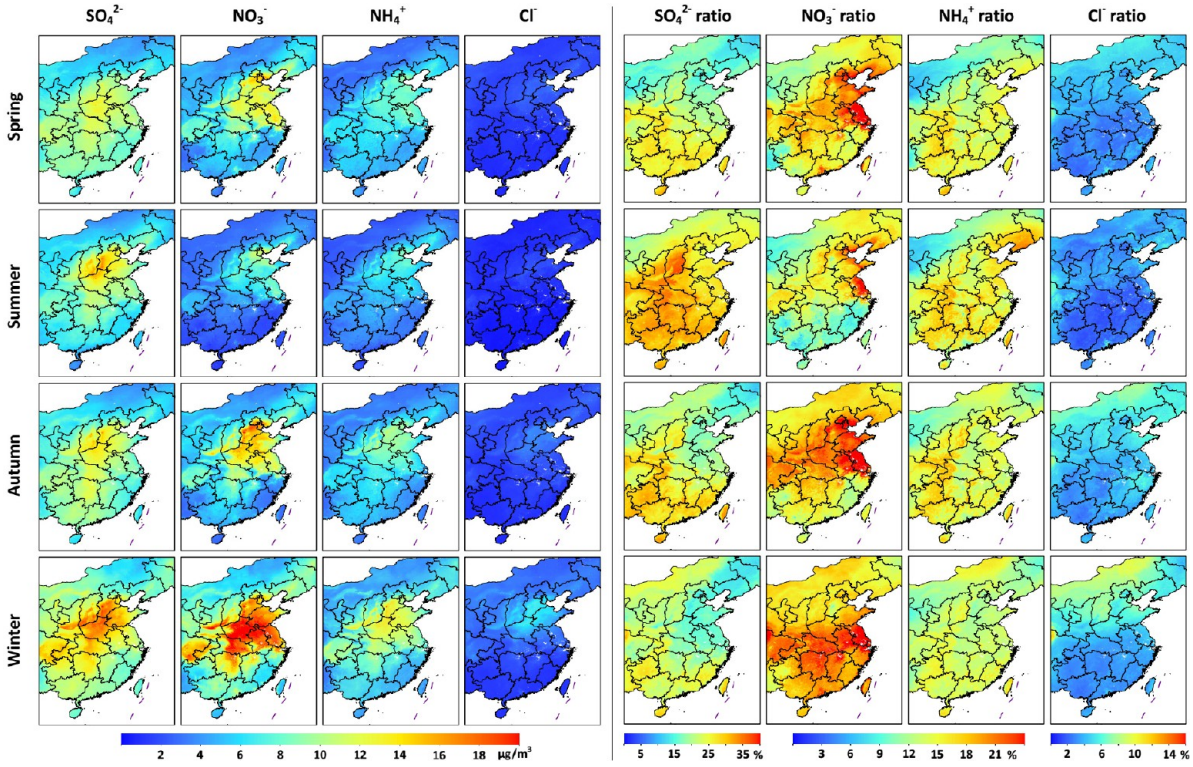

Figure 3. Spatial distributions of seasonal mean 1-km-resolution $PM_{2.5}$ inorganic components ($\mu g/m^3$, left set of panels) and composition-to-$PM_{2.5}$ ratios (%, right set of panels) of SO_4^{2-}, NO_3^-, NH_4^+, and Cl^- in eastern China averaged over the period 2013−2020.

national-scale daily estimates agree well with ground measurements, with out-of-sample CV-R^2 values of 0.74, 0.75, 0.71, and 0.66, and low RMSEs (MAEs) of 6.0 (3.3), 6.6 (3.8), 4.3 (2.4), and 2.3 (1.0) $\mu g/m^3$, for the four species, respectively. Spatially and temporally based cross-validations illustrate similar spatial patterns between daily retrievals and observations for $PM_{2.5}$ components at the individual-site scale but with an overall worse performance (Figures S5 and S6). A similar conclusion can be drawn regarding the national accuracy, with overall decreasing out-of-station CV-R^2 values of 0.65, 0.67, 0.62, and 0.48, and increasing RMSEs (MAEs) of 6.9 (3.8), 7.6 (4.4), 4.9 (2.8), and 2.9 (1.3) $\mu g/m^3$ for SO_4^{2-}, NO_3^-, NH_4^+, and Cl^-, respectively. The out-of-day CV results are comparable, with close CV-R^2 values of 0.66, 0.66, 0.65, and 0.55, and RMSEs (MAEs) of 6.8 (3.8), 7.7 (4.5), 4.7 (2.7), and 2.6 (1.2) $\mu g/m^3$, for the four species, respectively. They are notably better at monthly (e.g., R^2 = 0.84−0.87, 0.52−0.75, and 0.74−0.81, and RMSE = 1.3−3.6, 2.1−4.8, and 1.6−4.3 $\mu g/m^3$) and annual scales (R^2 = 0.87−0.91, 0.66−0.73, and 0.82−0.85, and RMSE = 0.5−1.9, 1.0−2.9, and 0.9−2.2 $\mu g/m^3$) based on syntheses of daily values at each monitoring station for sample, spatially, and temporally based CV results (Figures S7−S9).

3.2. Spatiotemporal Characteristics of $PM_{2.5}$ Composition. *3.2.1. Spatial Distribution and Proportion.* Lack or sparseness of ground observations in the period prior to 2013 or in western and northeastern China will inevitably incur large estimation uncertainties. Our analysis is thus mainly concentrated on eastern China, which has a much denser station network, during the period 2013−2020. In general, the four inorganic components have similar spatial patterns, with high concentrations centered over the North China Plain (NCP) (Figure 2), where SO_4^{2-} has much higher levels in nearby heavily industrialized zones, e.g., southern Hebei and Shanxi and northern Henan provinces. NO_3^- is mainly distributed over the economically developed urban agglomerations, e.g., the Beijing−Tianjin−Hebei (BTH) region and the Yangtze River Delta (YRD), and in major cities like Guangzhou and Wuhan. The spatial distribution of SO_4^{2-} reflects the dominant sources of SO_2, with coal combustion being a major source. Enhanced NO_3^- mainly occurs in cities and industrial centers, with large contributions from traffic and industrial emissions of NO_x.[59−61] NH_4^+ resembles the spatial pattern of the above two species but with a lower concentration because it mainly comes from agricultural emissions of NH_3 that neutralize SO_4^{2-} and NO_3^-.[61,62] By contrast, Cl^- concentrations are usually less than 2 $\mu g/m^3$ in eastern China, 3−5 times lower in population-weighted mean content than the other three inorganic components (Table S2). High values are mainly localized to heavily industrialized zones, such as BTH, and coastal areas, such as the Bohai Rim. These areas have abundant coarse-mode particles, e.g., sea salt, and fine particles produced by the combustion of fossil fuels like coal and biomass burning.[9]

Similar to $PM_{2.5}$, strong seasonal variations are revealed in our estimates (Figure 3). All inorganic components are at their highest levels in winter, especially in northern China, where coal burning for heating is the primary source,[63] compounded by the low boundary layer height.[64,65] By contrast, population-weighted mean concentrations are 1.4−3.3 times lower in summer than in winter in eastern China, especially NO_3^- in the Pearl River Delta (PRD, 4 times lower) (Table S2), mainly due to evaporative loss under high-temperature conditions.[66] There are also significant north−south differences due to different meteorological conditions, e.g., more abundant precipitation promoting the wet removal of particulate

https://doi.org/10.1021/acs.est.3c00272
Environ. Sci. Technol. XXXX, XXX, XXX−XXX

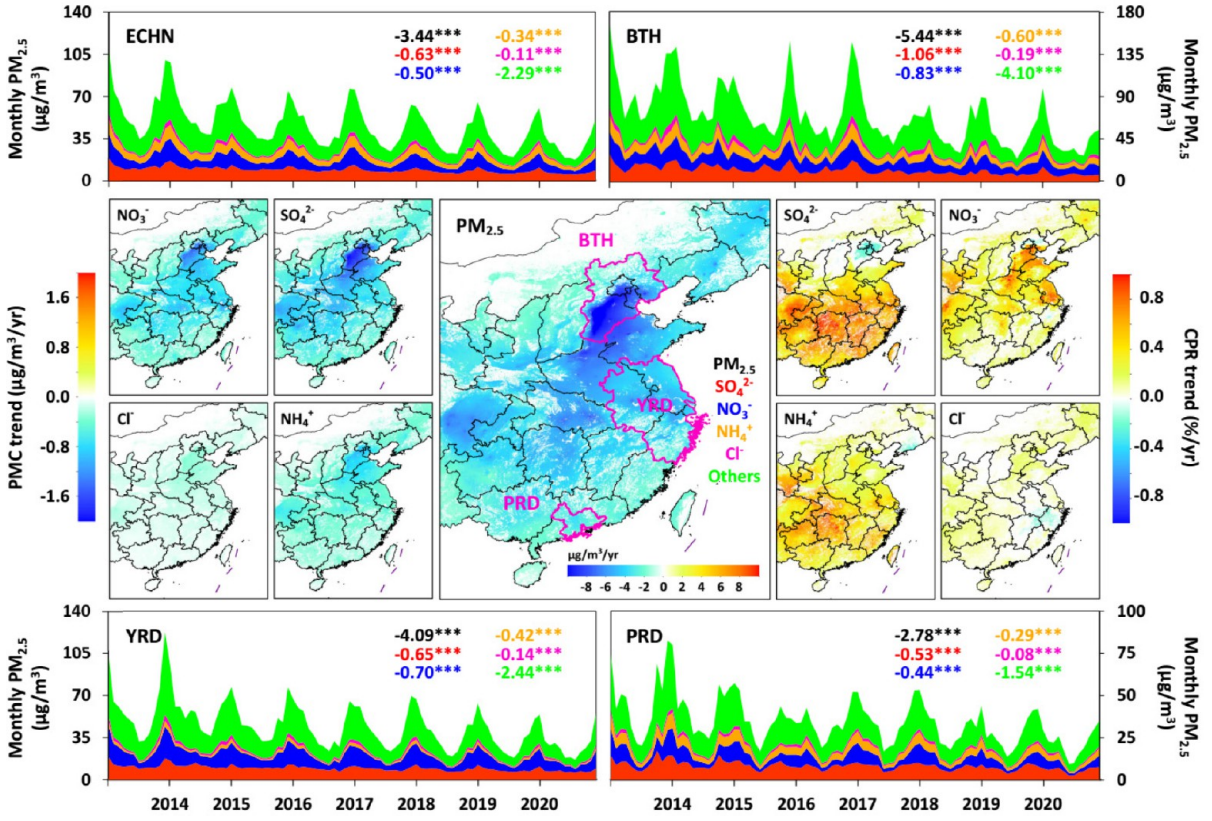

Figure 4. Spatial distributions of temporal trends of total $PM_{2.5}$ concentration ($\mu g/m^3$/year, central panel), $PM_{2.5}$ inorganic components (PMC, $\mu g/m^3$/year, set of panels to the left), and composition-to-$PM_{2.5}$ ratios (CPR, %/year, set of panels to the right) of SO_4^{2-}, NO_3^-, NH_4^+, and Cl^- in eastern China from 2013 to 2020. Note that only trends significant at the 95% ($p < 0.05$) confidence level in areas with population density >10 people per km^2 are shown. The line charts (top and bottom panels) show the time series of monthly $PM_{2.5}$ concentrations ($\mu g/m^3$) stacked by different chemical components from 2013 to 2020 in eastern China (ECHN) and three urban agglomerations (outlined by pink borders in the central panel): the Beijing−Tianjin−Hebei (BTH) region, the Yangtze River Delta (YRD), and the Pearl River Delta (PRD). Colored numbers give the temporal trends ($\mu g/m^3$/year) of different $PM_{2.5}$ species during the period 2013−2020, where *** indicates that the trends are significant at the 99.9% ($p < 0.001$) confidence level.

pollutants in southern China.[67,68] Spring and autumn have similar spatial patterns and pollution levels in eastern China and three typical urban agglomerations.

Regarding the proportions of inorganic components to total $PM_{2.5}$ (Figures 2 and 3), SO_4^{2-} accounts for 20.5% in eastern China and higher values in the south compared to the north, e.g., PRD is 1.4 times that of BTH. The SO_4^{2-} contribution reaches a maximum of 27.6% in summer (Table S3), especially in Shanxi Province, where high amounts of SO_2 are emitted from coal power plants.[41] The high temperature and stronger radiation also significantly enhance the chemical conversion from SO_2 to SO_4^{2-}.[10,39,69] NO_3^- accounts for 19.8% of the total $PM_{2.5}$ but has opposite seasonal changes to that of SO_4^{2-}, with the lowest value in summer (15%) and higher values in cold seasons in eastern China (Figure 3). This is explained by lower temperatures and more available NH_3-neutralizing sulfates that favor nitrate aerosol partitioning.[61,70] The annual NH_4^+ fraction is 13.9% in eastern China, showing a weaker seasonal contrast, with a somewhat higher value of ∼14% in summer, presumably due to higher NH_3 emissions from agricultural sources.[62,71] NH_4^+ resides mostly in the form of ammonium sulfate in summer but in ammonium nitrate in winter.[61] Annual and seasonal Cl^--to-$PM_{2.5}$ ratios are much smaller (average = 3−4.6%) than those of the other three inorganic species. In winter, the Cl^- contribution is higher in the northern and western vast regions and major urban areas due to the saline-alkali soils with dry meteorological conditions and large emissions from anthropogenic sources like coal combustion and residential biomass burning.[7−9] In general, the four main inorganic aerosols account for 58.1% of the total $PM_{2.5}$ in eastern China, of which the fraction of SIA is more than half (54.2%), reaching a maximum of 56.6% in summer while a minimum of 49.4% in winter. This dominant presence of SIAs calls upon the need for the persistent regulation of emissions of relevant precursor gases (i.e., SO_2, NO_x, and NH_3).

3.2.2. Temporal Variation and Trend. Steady declines are seen in the concentrations of the four inorganic components from 2013 to 2020 in eastern China at the annual rates of −0.63, −0.5, −0.34, and −0.11 $\mu g/m^3$ for SO_4^{2-}, NO_3^-, NH_4^+, and Cl^- ($p < 0.001$), respectively, especially in the BTH (−0.19 to −1.06 $\mu g/m^3$/year, $p < 0.001$) (Figure 4). This is highly consistent with the significant decline in total $PM_{2.5}$ (−2.78 to −5.44 $\mu g/m^3$/year, $p < 0.001$) attributed to substantial reductions in anthropogenic emissions benefiting from the implementation of new national environmental protection policies.[25,72] While the SO_4^{2-} contribution decreased sharply in Beijing, Tianjin, and surrounding areas, it increased rapidly in the south. The former decrease may have stemmed from the reduction of flue gas desulfurization from coal-fired boilers as coal combustion shifted to gas and electricity during the heating season in northern China.[73−75]

https://doi.org/10.1021/acs.est.3c00272
Environ. Sci. Technol. XXXX, XXX, XXX−XXX

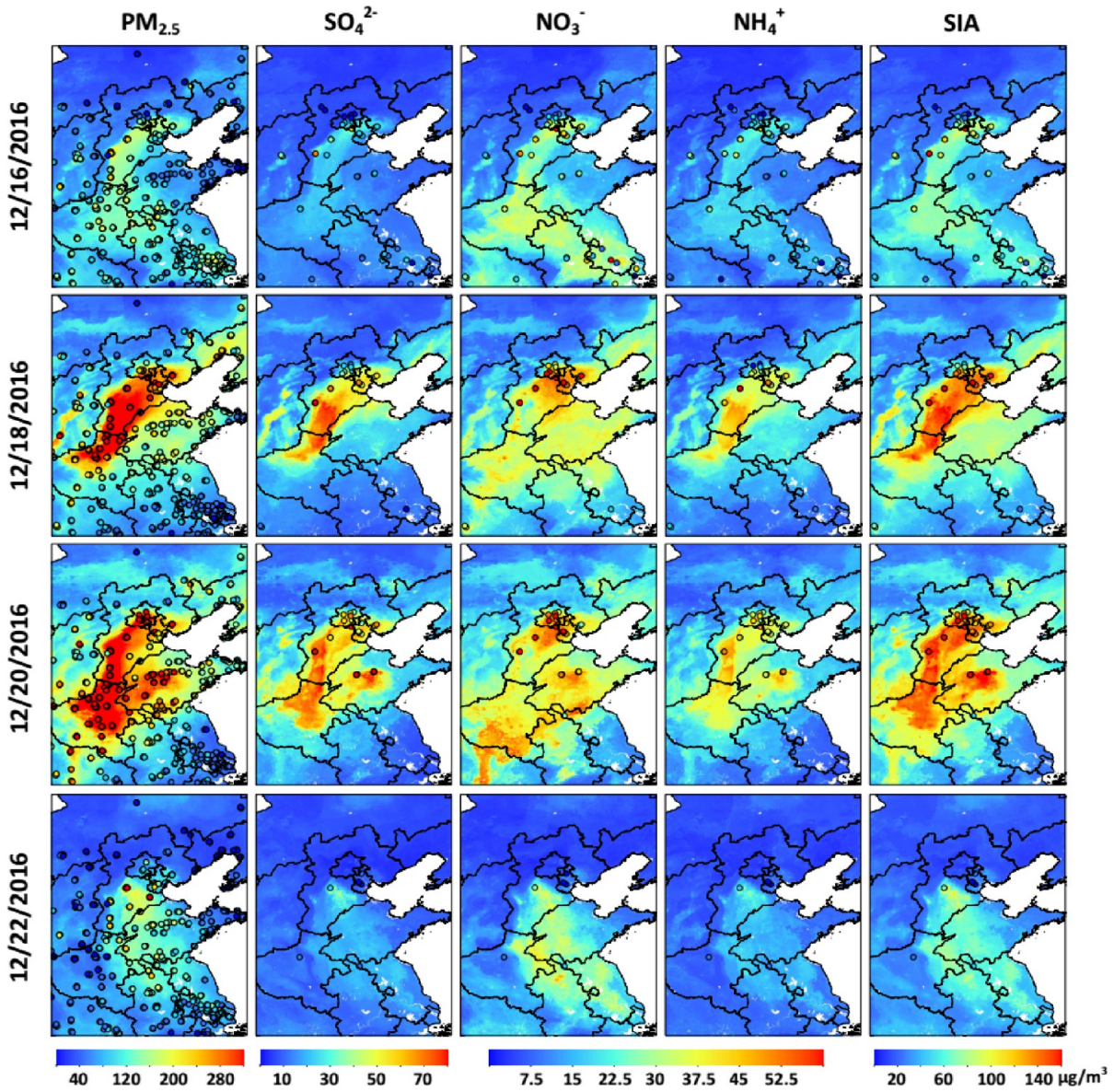

Figure 5. Typical example of satellite-derived (background maps) and ground-measured (colored dots) concentrations ($\mu g/m^3$) of $PM_{2.5}$, SO_4^{2-}, NO_3^-, NH_4^+, and secondary inorganic aerosols (SIAs) during a severe haze episode that occurred during December 16−22, 2016, in the North China Plain.

The proportion of NO_3^- also greatly increased in eastern China (0.36%/year, $p < 0.001$), especially since 2018 in BTH (0.81%/year, $p < 0.001$), highlighting the importance of NH_3 and NO_x controls for preventing future $PM_{2.5}$ pollution.[76] The NH_4^+-to-$PM_{2.5}$ ratio increased at a rate of 0.26% per year ($p < 0.001$) in eastern China as a result of the combined effects of changes in SO_4^{2-} and NO_3^-, which was higher in the south where the fractions of both anions increased. The Cl^- contribution overall did not change much over time. The increase in the inorganic-to-$PM_{2.5}$ ratio may reflect the faster decline in other components (−1.54 to −4.10 $\mu g/m^3$/year, $p < 0.001$), especially the significant reduction in primary $PM_{2.5}$ emissions (mostly organic carbon) following nationwide regulations after 2013.[59,60,72,77] Increased oxidation rates due to rising surface ozone levels could also speed up the formation of SIAs.[17,78] In addition, this may be partly attributed to reduced dust because coarse-mode aerosol particles (PM_{10}, $PM_{2.5-10}$) were observed to have declined considerably.[79,80]

In general, annual population-weighted mean concentrations of inorganic chemical composition dropped by 40−43% in eastern China from 2013 to 2020, with the largest declines in SO_4^{2-} in BTH (by 54%) and NO_3^- in the PRD (by 51%). Seasonally, SO_4^{2-} and NH_4^+ always decreased the most in summer in eastern China and three key regions (by 40−58% and 40−53%, respectively), while NO_3^- dropped the most in autumn by 45−52% (Figure S10). By contrast, the SIA contribution has been continuously increasing in eastern China during the last eight years (slope = 0.9%, $R^2 = 0.95$), with SO_4^{2-} still being the main secondary component in 2020 (population-weighted mean concentration = 6.9 $\mu g/m^3$ and SO_4^{2-}-to-$PM_{2.5}$ ratio = 21.7%), 8% higher in concentration and 1.6% higher in proportion than NO_3^-. Nevertheless, NO_3^- (slope = 0.36%, $R^2 = 0.96$) gradually approached SO_4^{2-} (slope = 0.29%, $R^2 = 0.86$). However, great contrasting regional differences exist, e.g., SO_4^{2-} remained dominant in the PRD (slope = 0.43%, $R^2 = 0.8$), while NO_3^- continuously

https://doi.org/10.1021/acs.est.3c00272
Environ. Sci. Technol. XXXX, XXX, XXX−XXX

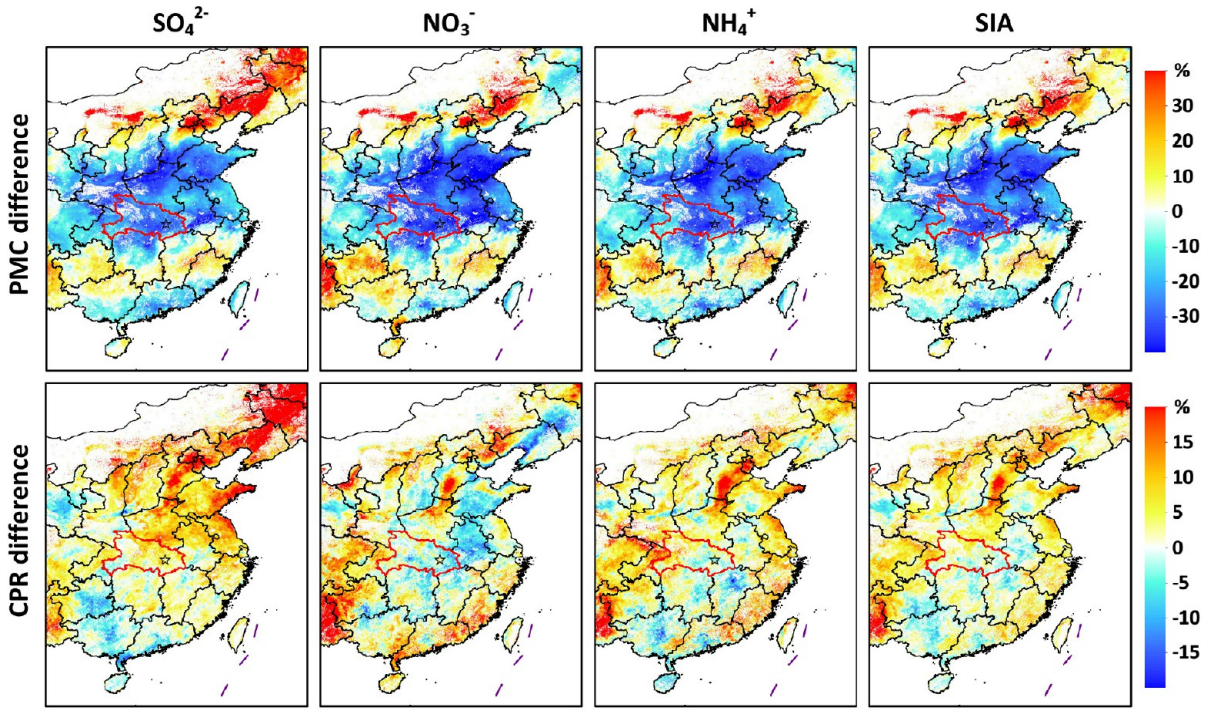

Figure 6. Relative differences (%) in $PM_{2.5}$ inorganic components (PMC, $\mu g/m^3$; top row) and composition-to-$PM_{2.5}$ ratios (CPR, %; bottom row) of SO_4^{2-}, NO_3^-, NH_4^+, and secondary inorganic aerosols (SIAs) from January 26 to February 17 (lockdown period) between the year of the COVID-19 epidemic (2020) and the normal year of 2019 in areas with population density >10 people per km^2 in eastern China. The red border and black star indicate Hubei Province and Wuhan City, respectively.

contributed the most in the YRD (slope = 0.43%, R^2 = 0.93). In BTH, the SO_4^{2-} contribution has been declining (slope = −0.13%, R^2 = 0.28), while the NO_3^- contribution has been rapidly rising (slope = 0.54%, R^2 = 0.9), becoming the dominant component since 2016 (Figure S11).

For policy implementations (Figure S12), the decline in $PM_{2.5}$ inorganic components was most dramatic during the Clean Air Action Plan (2013−2017) in eastern China, especially for SO_4^{2-} and NO_3^- (−0.72 and −0.60 $\mu g/m^3$/year, $p < 0.001$) (Table S4), with SO_2 and NO_x emissions falling by 59% and 21%, respectively.[60,81] The largest downward trends occurred in the NCP, consistent in spatial pattern with the changes in SO_2 and NO_2 concentrations at the surface.[41,82] However, during the Blue Sky Defense War (2018−2020), the downward trends slowed significantly. Areas with significant decreases shrank in size, mainly located in a handful of provinces (e.g., Beijing and Anhui) and urban agglomerations (e.g., PRD and YRD). In particular, SO_4^{2-} decreases occurred mainly in the core urban areas of central Shanxi province after 2018 due to the enforcement of the clean heating policy,[83−85] leading to a sharp reduction of 33% in surface SO_2 pollution.[41] Except for Cl^-, increases in the SIA proportion have accelerated overall in recent years. However, this was not seen in densely populated large cities like Beijing and Guangzhou, where the SIA proportion remained relatively stable from 2018 to 2020.

To validate the data reliability, we further compared national and regional $PM_{2.5}$ components and their ratios to total $PM_{2.5}$ calculated from surface observations (Tables S2 and S3). They are highly consistent, with little differences at both annual and seasonal levels. However, specific differences exist with average results from satellite retrievals, increasing as the region expands, e.g., eastern China, caused by significant differences in spatial representations.[25] Also, considering the large difference in sampling time between satellite-derived and ground-based observations, to be a fair comparison, we calculated their temporal trends with collocated data at each site (Figure S13). Results illustrate that our data set can accurately capture the variations of aerosol components (R^2 = 0.85) and reproduce well the changes in the proportion of $PM_{2.5}$ species (R^2 = 0.8).

3.2.3. Preliminary Investigation before 2013. Using our newly developed model, we also reconstructed historical data records of $PM_{2.5}$ chemical composition before 2013 to fill gaps in surface observations. Figure S14 shows the multiyear mean and annual temporal trends of the four inorganic components during 2000−2012. Their spatial patterns are particularly similar to those of 2013−2020 in eastern China, but 16%, 7%, 7%, and 13% higher in population-weighted mean concentrations of SO_4^{2-}, NO_3^-, NH_4^+, and Cl^-; differently, these four components show significant increasing trends at the annual rates of 0.15, 0.11, 0.07, and 0.03 $\mu g/m^3$ ($p < 0.001$), respectively. Highly polluted conditions and greater trends were observed in the NCP, associated with the significant increase in total $PM_{2.5}$, mainly due to more anthropogenic emissions of major pollutants caused by the rapid economic growth of the country.[25,39] Similar findings were also reported from previous model simulated studies.[39,77] Nevertheless, given the absence of historical observations, an independent analysis is needed to validate the reliability of data records estimated for the prior period.

3.3. Short-Term Changes in $PM_{2.5}$ Composition. *3.3.1. Haze Episode in the North China Plain.* The unique advantage of the daily seamless data set enables us to capture short-term episodes of heavy $PM_{2.5}$ pollution and analyze their causes with the help of chemical composition and its changes.

https://doi.org/10.1021/acs.est.3c00272
Environ. Sci. Technol. XXXX, XXX, XXX−XXX

Figure 5 illustrates a typical example of a severe wintertime haze episode that occurred during December 16−22, 2016, in the NCP. Our satellite-derived results are highly consistent with ground-based observations in terms of spatial pattern and amplitude of change. In particular, we filled spatial gaps, providing a seamless insight into this pollution episode where observations of $PM_{2.5}$ components were scarce. Here, overall low concentrations of $PM_{2.5}$ and inorganic components at the initial stage were captured as moderate pollution gradually formed near the major cities of Tianjin, Baoding, and Shijiazhuang. Subsequently, atmospheric pollution increased substantially, spreading rapidly to surrounding areas and finally to the entire NCP. Pollution reached its peak around December 20. Heavy pollution broadly affected several provinces, including Beijing, Tianjin, Hebei, Henan, Shandong, and even Hunan in southern China. Extremely high SO_4^{2-} hotspots are seen in heavily industrial cities like Shijiazhuang and Zibo, while NO_3^- hotspots were observed in core hub cities like Beijing and Tianjin mainly due to differences in main secondary pollutant emission sources (e.g., heavy industrial production and transportation) in local areas. After December 20, high concentrations of $PM_{2.5}$ and its components covered less area, finally dropping to background levels over the NCP.

A meta-analysis of multiple cases of heavy haze episodes from 2013 to 2020 (population-weighted mean $PM_{2.5}$ = 155.6 $\mu g/m^3$) illustrates that SIA fractions varied from 39.8% to 49.8%, with an average of 45.9%, of which NO_3^- and SO_4^{2-} were the two dominant components, accounting for 18.2% and 16.2% of the total $PM_{2.5}$ mass, respectively (Table S5). This suggests the important role of these two $PM_{2.5}$ components in regional pollution due to intensive anthropogenic emissions.[86] The continuous growth of SIA fractions (slope = 1.46%, R^2 = 0.87) became the main driver for winter haze in the NCP. In particular, NO_3^- (slope = 0.96%, R^2 = 0.72) became increasingly prominent over SO_4^{2-} (slope = 0.17%, R^2 = 0.18), with their rapid rises proving to be the key factors for the explosive growth of $PM_{2.5}$ pollution.[87,88]

3.3.2. Impacts of the COVID-19 Lockdown. This data set allows us to quantify changes in $PM_{2.5}$ composition more accurately during dramatic short-term events at a fine scale and investigate their influential factors and mechanisms. Figure 6 compares changes in SIA components and proportions during the COVID-19 lockdown in eastern China, where the former significantly decreased by 16.8% (especially NO_3^- by 19.7%) and the latter increased by 3.5% (especially SO_4^{2-} by 7.3%) as a whole (Table S6). The spatial patterns are striking: drastic declines of more than 20% in all SIA components in central (e.g., Henan, Hubei, Shandong, Jiangsu, and Anhui) and southern (e.g., Guangdong) China, in contrast to significant increases of more than 40% in the north and northeast (e.g., Beijing, Tianjin, northeastern Hebei, and western Liaoning) and parts of the southeast and southwest. The main reason was strict domestic restrictions on industry and transportation that sharply reduced anthropogenic emissions, e.g., NO_x and SO_2, by 36% and 27%, respectively.[54,89,90] Adverse meteorological conditions, which offset or even reversed the effect of anthropogenic emissions on air quality, may explain the anomaly in the north.[91−94] By contrast, the ratios of SIA components to $PM_{2.5}$ increased across most of the mapping domain, especially in the north, with the exception of the PRD, where they decreased (Table S6). Regarding the NO_3^- fraction, opposite declines were observed in the worst-hit areas by the epidemic, i.e., Hubei province (↓ 2.4%) and surrounding areas (e.g., Anhui), due to rapid reductions in NO_x, CO, and VOC emissions. These led to a significant increase in surface ozone in northern China, saturating NO_x[95] and greatly enhancing the atmospheric oxidation capacity and the formation of secondary $PM_{2.5}$. For the NO_x-controlled area in southern China, the impact was the opposite.[17,96,97]

3.4. Comparison with Related Data Sets and Previous Studies. We first compared our data set with model simulations of $PM_{2.5}$ inorganic composition by collecting daily mean surface mass concentrations (kg m^{-3}) of SO_4^{2-}, NO_3^-, NH_4^+, and Cl^- from the GEOS-FP reanalysis and SO_4^{2-} and Cl^- from the MERRA2 reanalysis and validating against ground-based measurements from 2013 to 2020 in China (Figure S15). Besides coarse spatial resolutions (0.25°−0.625°), the chemical transport models did a poorer job in simulating $PM_{2.5}$ inorganic components, seriously underestimating the concentrations with stronger deviations, especially for SO_4^{2-} and Cl^- (e.g., $R^2 \leq 0.05$, slope ≤0.18). By contrast, our estimates improved the spatial resolution drastically by 25−63 times, increasing the correlations by 3−66 times and reducing the RMSE (MAE) values by 36−61% (40−65%) compared to chemical-model simulations, benefiting from the integration of big data and deep learning.

Two previous estimates of SIAs over China were derived from chemical transport modeling data with composition-specific conversions based on satellite AOD or $PM_{2.5}$ estimates but showed poor agreement with in situ measurements (R^2 = 0.38−0.56) for daily SIA estimates of SO_4^{2-}, NO_3^-, and NH_4^+ components at a 10-km resolution.[39,40] We also made a comparison with an open-access source, namely, Tracking Air Pollution (TAP) in China (http://tapdata.org.cn),[77] at the same monitoring stations over the same period (2013−2020), showing an average R^2 of 0.37−0.44 and RMSE of 6.4−10.4 $\mu g/m^3$ between daily estimates (10 km) and surface observations of SO_4^{2-}, NO_3^-, and NH_4^+ components (Figure S16). Compared to these studies, our new ChinaHighPMC data set has a ten times higher spatial resolution (1 km) and higher data quality (R^2 = 0.71−0.75 and RMSE = 4.2−6.7 $\mu g/m^3$) for the three SIA components; our data set also includes another inorganic component, i.e., Cl^-. One reason for the better performance of our model is that it relies on a denser network of direct ground-based observations rather than on the more dependent chemical model conversion. Another reason is the stronger data-mining ability of our deep-learning model.

3.5. Limitations and Prospects. Despite the encouraging results, limitations still exist. The in situ $PM_{2.5}$ composition network is much sparser than that of total $PM_{2.5}$, resulting in insufficient spatial representation. Some input parameters simulated by chemical transport models also suffer from large biases in regions without observations. They undoubtedly bring significant uncertainties to our estimates. The current study only focuses on the inorganic composition of $PM_{2.5}$, while a future study will be investigated focusing on the organic parts as well as black carbon, which may have greater toxicity and environmental effects. More detailed satellite-based aerosol information, such as those (e.g., aerosol shape, size, and extinction) conveyed in NASA's Multi-angle Imaging SpectroRadiometer (MISR) products, will be explored to improve the estimation in the future.

https://doi.org/10.1021/acs.est.3c00272
Environ. Sci. Technol. XXXX, XXX, XXX−XXX

■ ASSOCIATED CONTENT

Data Availability Statement

The ChinHighAirPollutants (CHAP) data set is available at https://weijing-rs.github.io/product.html, and the China-HighPMC data set is available at 10.5281/zenodo.5919481.

Supporting Information

The Supporting Information is available free of charge at https://pubs.acs.org/doi/10.1021/acs.est.3c00272.

Additional experimental details, materials, and methods, including monitor location; model framework and feature importance; spatiotemporal variation, validation, and comparison of $PM_{2.5}$ composition; summary of the data sources; and statistics of concentrations and changes of $PM_{2.5}$ composition and its ratio (PDF)

■ AUTHOR INFORMATION

Corresponding Authors

Zhanqing Li − *Department of Atmospheric and Oceanic Science, Earth System Science Interdisciplinary Center, University of Maryland, College Park, Maryland 20742, United States;* orcid.org/0000-0001-6737-382X; Email: zli@atmos.umd.edu

Xi Chen − *National Institute of Environmental Health, Chinese Center for Disease Control and Prevention, Beijing 100050, China*; Email: chenxi@nieh.chinacdc.cn

Jing Wei − *Department of Atmospheric and Oceanic Science, Earth System Science Interdisciplinary Center, University of Maryland, College Park, Maryland 20742, United States;* orcid.org/0000-0002-8803-7056; Email: weijing_rs@163.com

Authors

Chi Li − *Department of Energy, Environmental and Chemical Engineering, Washington University in St. Louis, St. Louis, Missouri 63130, United States;* orcid.org/0000-0002-8992-7026

Yele Sun − *State Key Laboratory of Atmospheric Boundary Physics and Atmospheric Chemistry, Institute of Atmospheric Physics, Chinese Academy of Sciences, Beijing 100029, China;* orcid.org/0000-0003-2354-0221

Jun Wang − *Department of Chemical and Biochemical Engineering, Iowa Technology Institute, University of Iowa, Iowa 52242, United States;* orcid.org/0000-0002-7334-0490

Alexei Lyapustin − *Laboratory for Atmospheres, NASA Goddard Space Flight Center, Greenbelt, Maryland 20771, United States*

Guy Pierre Brasseur − *Max Planck Institute for Meteorology, Hamburg 20146, Germany; National Center for Atmospheric Research, Boulder, Colorado 80307, United States*

Mengjiao Jiang − *Max Planck Institute for Meteorology, Hamburg 20146, Germany; School of Atmospheric Sciences, Chengdu University of Information Technology, Chengdu 610225, China*

Lin Sun − *College of Geodesy and Geomatics, Shandong University of Science and Technology, Qingdao 266590, China*

Tao Wang − *Department of Civil and Environmental Engineering, The Hong Kong Polytechnic University, Hong Kong 999077, China*

Chang Hoon Jung − *Department of Health Management, Kyungin Women's University, Incheon 21041, Korea;* orcid.org/0000-0003-0221-6764

Bing Qiu − *Civil Aviation Medical Center, Civil Aviation Administration of China, Beijing 100123, China*

Cuilan Fang − *Jiulongpo Center for Disease Control and Prevention, Chongqing 400039, China*

Xuhui Liu − *Taiyuan Center for Disease Control and Prevention, Taiyuan 030015, China*

Jinrui Hao − *Taiyuan Center for Disease Control and Prevention, Taiyuan 030015, China*

Yan Wang − *Harbin Center for Disease Control and Prevention, Harbin 150010, China*

Ming Zhan − *Pudong Center for Disease Control and Prevention, Shanghai 200120, China*

Xiaohong Song − *Shimadzu (China) Co., Ltd., Beijing 100020, China*

Yuewei Liu − *Department of Epidemiology, School of Public Health, Sun Yat-sen University, Guangzhou, Guangdong 510080, China;* orcid.org/0000-0001-5970-4262

Complete contact information is available at: https://pubs.acs.org/10.1021/acs.est.3c00272

Notes

The authors declare no competing financial interest.

■ ACKNOWLEDGMENTS

J. Wei and Z. Li were supported by the NASA Earth Sciences' Applied Science Program (Grant number: 80NSSC21K1980). A. Lyapustin was supported by NASA MODIS maintenance program and NASA NNH20ZDA001N-SNPPSP funding. The National Center for Atmospheric Research is sponsored by the National Science Foundation. The work was also partially supported by the National Natural Science Foundation of China (Grant numbers: U1633130 and 41771435), the Hainan Provincial Natural Science Foundation of China (Grant number: 821MS150), the Joint Medical Research Project of Chongqing Municipal Health Commission and Chongqing Science and Technology Bureau (Frant number: 2019MSXM069), and the First batch of key Disciplines on Public Health in Chongqing. The authors greatly thank Wenhao Xue from Qingdao University, Yuying Wang from Nanjing University of Information Science & Technology, and Maureen Cribb from the University of Maryland for their help in data processing, paper reviewing, and editing. The authors offer their sincere thanks to all the scientific researchers from the ground monitoring stations, such as members of the Jiulongpo Center for Disease Control and Prevention and the Hainan Provincial Center for Disease Control and Prevention, particularly Lun Xiao, Shang Li, Chongjun Ran, Shushu Lan, Nanyan Li, Changhua He, Yue Zeng, Xi Yang, and Dan Feng, for their support in aerosol sampling. Our gratitude also goes to Shimadzu (China) Co., Ltd., particularly to Bin Li and Feng Ji, for their technical support in sample analyses.

■ REFERENCES

(1) Murray, C. J. L.; Aravkin, A. Y.; Zheng, P.; Abbafati, C.; Abbas, K. M.; Abbasi-Kangevari, M.; Abd-Allah, F.; Abdelalim, A.; Abdollahi, M.; Abdollahpour, I. Global burden of 87 risk factors in 204 countries and territories, 1990−2019: a systematic analysis for the Global Burden of Disease Study 2019. *Lancet* **2020**, *396* (10258), 1223−1249.

(2) Zheng, M.; Yan, C.; Wang, S.; He, K.; Zhang, Y. Understanding $PM_{2.5}$ sources in China: challenges and perspectives. *Nat. Sci. Rev.* **2017**, *4* (6), 801−803.
(3) Fu, X.; Wang, S.; Chang, X.; Cai, S.; Xing, J.; Hao, J. Modeling analysis of secondary inorganic aerosols over China: pollution characteristics, and meteorological and dust impacts. *Sci. Rep.* **2016**, *6* (1), 35992.
(4) Meng, F.; Zhang, Y.; Kang, J.; Heal, M. R.; Reis, S.; Wang, M.; Liu, L.; Wang, K.; Yu, S.; Li, P.; Wei, J.; Hou, Y.; Zhang, Y.; Liu, X.; Cui, Z.; Xu, W.; Zhang, F. Trends in secondary inorganic aerosol pollution in China and its responses to emission controls of precursors in wintertime. *Atmos. Chem. Phys.* **2022**, *22* (9), 6291−6308.
(5) Wang, X.; Jacob, D. J.; Fu, X.; Wang, T.; Breton, M. L.; Hallquist, M.; Liu, Z.; McDuffie, E. E.; Liao, H. Effects of Anthropogenic Chlorine on $PM_{2.5}$ and Ozone Air Quality in China. *Environ. Sci. Technol.* **2020**, *54* (16), 9908−9916.
(6) Gunthe, S. S.; Liu, P.; Panda, U.; Raj, S. S.; Sharma, A.; Darbyshire, E.; Reyes-Villegas, E.; Allan, J.; Chen, Y.; Wang, X.; Song, S.; Pöhlker, M. L.; Shi, L.; Wang, Y.; Kommula, S. M.; Liu, T.; Ravikrishna, R.; McFiggans, G.; Mickley, L. J.; Martin, S. T.; Pöschl, U.; Andreae, M. O.; Coe, H. Enhanced aerosol particle growth sustained by high continental chlorine emission in India. *Nat. Geosci.* **2021**, *14* (2), 77−84.
(7) Fu, X.; Wang, T.; Wang, S.; Zhang, L.; Cai, S.; Xing, J.; Hao, J. Anthropogenic Emissions of Hydrogen Chloride and Fine Particulate Chloride in China. *Environ. Sci. Technol.* **2018**, *52* (3), 1644−1654.
(8) Peng, X.; Wang, W.; Xia, M.; Chen, H.; Ravishankara, A. R.; Li, Q.; Saiz-Lopez, A.; Liu, P.; Zhang, F.; Zhang, C.; Xue, L.; Wang, X.; George, C.; Wang, J.; Mu, Y.; Chen, J.; Wang, T. An unexpected large continental source of reactive bromine and chlorine with significant impact on wintertime air quality. *Nat. Sci. Rev.* **2021**, *8* (7), nwaa304.
(9) Yang, X.; Wang, T.; Xia, M.; Gao, X.; Li, Q.; Zhang, N.; Gao, Y.; Lee, S.; Wang, X.; Xue, L.; Yang, L.; Wang, W. Abundance and origin of fine particulate chloride in continental China. *Sci. Total Environ.* **2018**, *624*, 1041−1051.
(10) Li, C.; Martin, R. V.; van Donkelaar, A.; Boys, B. L.; Hammer, M. S.; Xu, J.-W.; Marais, E. A.; Reff, A.; Strum, M.; Ridley, D. A.; Crippa, M.; Brauer, M.; Zhang, Q. Trends in Chemical Composition of Global and Regional Population-Weighted Fine Particulate Matter Estimated for 25 Years. *Environ. Sci. Technol.* **2017**, *51* (19), 11185−11195.
(11) van Donkelaar, A.; Martin, R. V.; Li, C.; Burnett, R. T. Regional Estimates of Chemical Composition of Fine Particulate Matter Using a Combined Geoscience-Statistical Method with Information from Satellites, Models, and Monitors. *Environ. Sci. Technol.* **2019**, *53* (5), 2595−2611.
(12) Larssen, T.; Lydersen, E.; Tang, D.; et al. Acid Rain in China. *Environ. Sci. Technol.* **2006**, *40* (2), 418−425.
(13) Shi, Z.; Zhang, J.; Xiao, Z.; Lu, T.; Ren, X.; Wei, H. Effects of acid rain on plant growth: A meta-analysis. *J. Environ. Manage.* **2021**, *297*, 113213.
(14) An, Z.; Huang, R.-J.; Zhang, R.; Tie, X.; Li, G.; Cao, J.; Zhou, W.; Shi, Z.; Han, Y.; Gu, Z.; Ji, Y. Severe haze in northern China: A synergy of anthropogenic emissions and atmospheric processes. *Proc. Natl. Acad. Sci. U.S.A* **2019**, *116* (18), 8657−8666.
(15) Huang, R.-J.; Zhang, Y.; Bozzetti, C.; Ho, K.-F.; Cao, J.-J.; Han, Y.; Daellenbach, K. R.; Slowik, J. G.; Platt, S. M.; Canonaco, F.; Zotter, P.; Wolf, R.; Pieber, S. M.; Bruns, E. A.; Crippa, M.; Ciarelli, G.; Piazzalunga, A.; Schwikowski, M.; Abbaszade, G.; Schnelle-Kreis, J.; Zimmermann, R.; An, Z.; Szidat, S.; Baltensperger, U.; Haddad, I. E.; Prévôt, A. S. H. High secondary aerosol contribution to particulate pollution during haze events in China. *Nature* **2014**, *514* (7521), 218−222.
(16) Aubry, T.; Staunton-Sykes, J.; Marshall, L.; Haywood, J.; Abraham, N.; Schmidt, A. Climate change modulates the stratospheric volcanic sulfate aerosol lifecycle and radiative forcing from tropical eruptions. *Nat. Commun.* **2021**, *12*, 4708.
(17) Wei, J.; Li, Z.; Li, K.; Dickerson, R. R.; Pinker, R. T.; Wang, J.; Liu, X.; Sun, L.; Xue, W.; Cribb, M. Full-coverage mapping and spatiotemporal variations of ground-level ozone (O_3) pollution from 2013 to 2020 across China. *Remote Sens. Environ.* **2022**, *270*, 112775.
(18) Achilleos, S.; Kioumourtzoglou, M.-A.; Wu, C.-D.; Schwartz, J. D.; Koutrakis, P.; Papatheodorou, S. I. Acute effects of fine particulate matter constituents on mortality: A systematic review and meta-regression analysis. *Environ. Int.* **2017**, *109*, 89−100.
(19) Chen, J.; Li, C.; Ristovski, Z.; Milic, A.; Gu, Y.; Islam, M. S.; Wang, S.; Hao, J.; Zhang, H.; He, C.; Guo, H.; Fu, H.; Miljevic, B.; Morawska, L.; Thai, P.; Lam, Y. F.; Pereira, G.; Ding, A.; Huang, X.; Dumka, U. C. A review of biomass burning: Emissions and impacts on air quality, health and climate in China. *Sci. Total Environ.* **2017**, *579*, 1000−1034.
(20) Reid, C. E.; Brauer, M.; Johnston, F. H.; Jerrett, M.; Balmes, J. R.; Elliott, C. T. Critical Review of Health Impacts of Wildfire Smoke Exposure. *Environ. Health Perspect.* **2016**, *124* (9), 1334−1343.
(21) Sinharay, R.; Gong, J.; Barratt, B.; Ohman-Strickland, P.; Ernst, S.; Kelly, F. J.; Zhang, J.; Collins, P.; Cullinan, P.; Chung, K. F. Respiratory and cardiovascular responses to walking down a traffic-polluted road compared with walking in a traffic-free area in participants aged 60 years and older with chronic lung or heart disease and age-matched healthy controls: a randomised, crossover study. *Lancet* **2018**, *391* (10118), 339−349.
(22) Brugge, D.; Durant, J. L.; Rioux, C. Near-highway pollutants in motor vehicle exhaust: A review of epidemiologic evidence of cardiac and pulmonary health risks. *Environ. Health: Glob.* **2007**, *6* (1), 23.
(23) Gao, J.; Woodward, A.; Vardoulakis, S.; Kovats, S.; Wilkinson, P.; Li, L.; Xu, L.; Li, J.; Yang, J.; Li, J.; Cao, L.; Liu, X.; Wu, H.; Liu, Q. Haze, public health and mitigation measures in China: A review of the current evidence for further policy response. *Sci. Total Environ.* **2017**, *578*, 148−157.
(24) Yang, J.; Zhou, M.; Yin, P.; Li, M.; Ou, C.-Q.; Gu, S.; Liu, Q. Mortality as a function of dust-haze in China: a multi-city time-series study. *Lancet* **2016**, *388*, S19.
(25) Wei, J.; Li, Z.; Lyapustin, A.; Sun, L.; Peng, Y.; Xue, W.; Su, T.; Cribb, M. Reconstructing 1-km-resolution high-quality $PM_{2.5}$ data records from 2000 to 2018 in China: spatiotemporal variations and policy implications. *Remote Sens. Environ.* **2021**, *252*, 112136.
(26) Yang, F.; Tan, J.; Zhao, Q.; Du, Z.; He, K.; Ma, Y.; Duan, F.; Chen, G.; Zhao, Q. Characteristics of PM2.5 speciation in representative megacities and across China. *Atmos. Chem. Phys.* **2011**, *11* (11), 5207−5219.
(27) Liu, Z.; Gao, W.; Yu, Y.; Hu, B.; Xin, J.; Sun, Y.; Wang, L.; Wang, G.; Bi, X.; Zhang, G.; Xu, H.; Cong, Z.; He, J.; Xu, J.; Wang, Y. Characteristics of $PM_{2.5}$ mass concentrations and chemical species in urban and background areas of China: emerging results from the CARE-China network. *Atmos. Chem. Phys.* **2018**, *18* (12), 8849−8871.
(28) Feng, X.; Tian, Y.; Xue, Q.; Song, D.; Huang, F.; Feng, Y. Measurement report: Spatiotemporal and policy-related variations of $PM_{2.5}$ composition and sources during 2015−2019 at multiple sites in a Chinese megacity. *Atmos. Chem. Phys.* **2021**, *21* (21), 16219−16235.
(29) Sun, Y. L.; Wang, Z. F.; Du, W.; Zhang, Q.; Wang, Q. Q.; Fu, P. Q.; Pan, X. L.; Li, J.; Jayne, J.; Worsnop, D. R. Long-term real-time measurements of aerosol particle composition in Beijing, China: seasonal variations, meteorological effects, and source analysis. *Atmos. Chem. Phys.* **2015**, *15* (17), 10149−10165.
(30) Wang, Y.; Li, Z.; Wang, Q.; Jin, X.; Yan, P.; Cribb, M.; Li, Y.; Yuan, C.; Wu, H.; Wu, T.; Ren, R.; Cai, Z. Enhancement of secondary aerosol formation by reduced anthropogenic emissions during Spring Festival 2019 and enlightenment for regional $PM_{2.5}$ control in Beijing. *Atmos. Chem. Phys.* **2021**, *21* (2), 915−926.
(31) Miao, R.; Chen, Q.; Zheng, Y.; Cheng, X.; Sun, Y.; Palmer, P. I.; Shrivastava, M.; Guo, J.; Zhang, Q.; Liu, Y.; Tan, Z.; Ma, X.; Chen, S.; Zeng, L.; Lu, K.; Zhang, Y. Model bias in simulating major chemical components of $PM_{2.5}$ in China. *Atmos. Chem. Phys.* **2020**, *20* (20), 12265−12284.

https://doi.org/10.1021/acs.est.3c00272
Environ. Sci. Technol. XXXX, XXX, XXX−XXX

(32) Philip, S.; Martin, R. V.; van Donkelaar, A.; Lo, J. W.-H.; Wang, Y.; Chen, D.; Zhang, L.; Kasibhatla, P. S.; Wang, S.; Zhang, Q.; Lu, Z.; Streets, D. G.; Bittman, S.; Macdonald, D. J. Global Chemical Composition of Ambient Fine Particulate Matter for Exposure Assessment. *Environ. Sci. Technol.* **2014**, *48* (22), 13060−13068.
(33) Weagle, C. L.; Snider, G.; Li, C.; van Donkelaar, A.; Philip, S.; Bissonnette, P.; Burke, J.; Jackson, J.; Latimer, R.; Stone, E.; Abboud, I.; Akoshile, C.; Anh, N. X.; Brook, J. R.; Cohen, A.; Dong, J.; Gibson, M. D.; Griffith, D.; He, K. B.; Holben, B. N.; Kahn, R.; Keller, C. A.; Kim, J. S.; Lagrosas, N.; Lestari, P.; Khian, Y. L.; Liu, Y.; Marais, E. A.; Martins, J. V.; Misra, A.; Muliane, U.; Pratiwi, R.; Quel, E. J.; Salam, A.; Segev, L.; Tripathi, S. N.; Wang, C.; Zhang, Q.; Brauer, M.; Rudich, Y.; Martin, R. V. Global Sources of Fine Particulate Matter: Interpretation of $PM_{2.5}$ Chemical Composition Observed by SPARTAN using a Global Chemical Transport Model. *Environ. Sci. Technol.* **2018**, *52* (20), 11670−11681.
(34) Li, H.; Yang, Y.; Wang, H.; Wang, P.; Yue, X.; Liao, H. Projected Aerosol Changes Driven by Emissions and Climate Change Using a Machine Learning Method. *Environ. Sci. Technol.* **2022**, *56* (7), 3884−3893.
(35) Meng, X.; Garay, M. J.; Diner, D. J.; Kalashnikova, O. V.; Xu, J.; Liu, Y. Estimating $PM_{2.5}$ speciation concentrations using prototype 4.4 km-resolution MISR aerosol properties over Southern California. *Atmos. Environ.* **2018**, *181*, 70−81.
(36) Di, Q.; Koutrakis, P.; Schwartz, J. A hybrid prediction model for $PM_{2.5}$ mass and components using a chemical transport model and land use regression. *Atmos. Environ.* **2016**, *131*, 390−399.
(37) Bergen, S.; Sheppard, L.; Sampson, P. D.; Kim, S.-Y.; Richards, M.; Vedal, S.; Kaufman, J. D.; Szpiro, A. A. A National Prediction Model for $PM_{2.5}$ Component Exposures and Measurement Error−Corrected Health Effect Inference. *Environ. Health Perspect.* **2013**, *121* (9), 1017−1025.
(38) Kim, S.-Y.; Sheppard, L.; Bergen, S.; Szpiro, A. A.; Sampson, P. D.; Kaufman, J. D.; Vedal, S. Prediction of fine particulate matter chemical components with a spatio-temporal model for the Multi-Ethnic Study of Atherosclerosis cohort. *J. Expo. Sci. Env. Epid.* **2016**, *26* (5), 520−528.
(39) Geng, G.; Zhang, Q.; Tong, D.; Li, M.; Zheng, Y.; Wang, S.; He, K. Chemical composition of ambient $PM_{2.5}$ over China and relationship to precursor emissions during 2005−2012. *Atmos. Chem. Phys.* **2017**, *17* (14), 9187−9203.
(40) Si, Y.; Li, S.; Chen, L.; Yu, C.; Zhu, W. Estimation of Satellite-Based SO_4^{2-} and NH_4^+ Composition of Ambient Fine Particulate Matter over China Using Chemical Transport Model. *Remote Sens.* **2017**, *9* (8), 817.
(41) Wei, J.; Li, Z.; Wang, J.; Li, C.; Gupta, P.; Cribb, M. Ground-level gaseous pollutants (NO_2, SO_2, and CO) in China: daily seamless mapping and spatiotemporal variations. *Atmos. Chem. Phys.* **2023**, *23* (2), 1511−1532.
(42) Chen, X.; Zheng, L.; Wang, G.; Ji, F.; Gao, H.; Zhu, Y.; Xu, D. Assessment of pollution and contents of water-soluble ions in airborne submicrometer particles using ion chromatography. *Environ. Chem.* **2019**, *38*, 704−707.
(43) Chen, X.; Qiu, B.; Zou, Q.; Qiu, T.; Li, R.; Truong, A.; Qi, Y.; Liu, T.; Han, L.; Liu, T.; Chang, J.; Sun, Q.; Zhu, Y.; Xu, D. Source specific $PM_{2.5}$ associated with heart rate variability in the elderly with coronary heart disease: A community-based panel study. *Chemosphere* **2020**, *260*, 127399.
(44) Lyapustin, A.; Wang, Y.; Korkin, S.; Huang, D. MODIS Collection 6 MAIAC algorithm. *Atmos. Meas. Technol.* **2018**, *11* (10), 5741−5765.
(45) Song, J.; Du, P.; Yi, W.; Wei, J.; Fang, J.; Pan, R.; Zhao, F.; Zhang, Y.; Xu, Z.; Sun, Q.; Liu, Y.; Chen, C.; Cheng, J.; Lu, Y.; Li, T.; Su, H.; Shi, X. Using an Exposome-Wide Approach to Explore the Impact of Urban Environments on Blood Pressure among Adults in Beijing-Tianjin-Hebei and Surrounding Areas of China. *Environ. Sci. Technol.* **2022**, *56* (12), 8395−8405.
(46) Ge, E.; Gao, J.; Wei, X.; Ren, Z.; Wei, J.; Liu, X.; Wang, X.; Zhong, J.; Lu, J.; Tian, X.; Fei, F.; Chen, B.; Wang, X.; Peng, Y.; Luo, M.; Lei, J. Effect modification of greenness on $PM_{2.5}$ associated all-cause mortality in a multidrug-resistant tuberculosis cohort. *Thorax* **2022**, *77*, 1202−1209.
(47) Xu, H.; Guo, B.; Qian, W.; Ciren, Z.; Guo, W.; Zeng, Q.; Mao, D.; Xiao, X.; Wu, J.; Wang, X.; Wei, J.; Chen, G.; Li, S.; Guo, Y.; Meng, Q.; Zhao, X. Dietary Pattern and Long-Term Effects of Particulate Matter on Blood Pressure: A Large Cross-Sectional Study in Chinese Adults. *Hypertension* **2021**, *78* (1), 184−194.
(48) Li, X.; Xue, W.; Wang, K.; Che, Y.; Wei, J. Environmental regulation and synergistic effects of PM2.5 control in China. *J. Clean Prod.* **2022**, *337*, 130438.
(49) Jiang, Y.; Tian, S.; Xu, Z.; Gao, L.; Xiao, L.; Chen, S.; Xu, K.; Chang, J.; Luo, Z.; Shi, Z. Decoupling environmental impact from economic growth to achieve Sustainable Development Goals in China. *J. Environ. Manage.* **2022**, *312*, 114978.
(50) Inness, A.; Ades, M.; Agustí-Panareda, A.; Barré, J.; Benedictow, A.; Blechschmidt, A. M.; Dominguez, J. J.; Engelen, R.; Eskes, H.; Flemming, J.; Huijnen, V.; Jones, L.; Kipling, Z.; Massart, S.; Parrington, M.; Peuch, V. H.; Razinger, M.; Remy, S.; Schulz, M.; Suttie, M. The CAMS reanalysis of atmospheric composition. *Atmos. Chem. Phys.* **2019**, *19* (6), 3515−3556.
(51) Munoz-Sabater, J.; Dutra, E.; Agusti-Panareda, A.; Albergel, C.; Arduini, G.; Balsamo, G.; Boussetta, S.; Choulga, M.; Harrigan, S.; Hersbach, H.; Martens, B.; Miralles, D. G.; Piles, M.; Rodriguez-Fernandez, N. J.; Zsoter, E.; Buontempo, C.; Thepaut, J. N. ERA5-Land: a state-of-the-art global reanalysis dataset for land applications. *Earth Syst. Sci. Data* **2021**, *13* (9), 4349−4383.
(52) Hersbach, H.; Bell, B.; Berrisford, P.; Hirahara, S.; Horanyi, A.; Munoz-Sabater, J.; Nicolas, J.; Peubey, C.; Radu, R.; Schepers, D.; Simmons, A.; Soci, C.; Abdalla, S.; Abellan, X.; Balsamo, G.; Bechtold, P.; Biavati, G.; Bidlot, J.; Bonavita, M.; De Chiara, G.; Dahlgren, P.; Dee, D.; Diamantakis, M.; Dragani, R.; Flemming, J.; Forbes, R.; Fuentes, M.; Geer, A.; Haimberger, L.; Healy, S.; Hogan, R. J.; Holm, E.; Janiskova, M.; Keeley, S.; Laloyaux, P.; Lopez, P.; Lupu, C.; Radnoti, G.; de Rosnay, P.; Rozum, I.; Vamborg, F.; Villaume, S.; Thepaut, J. N. The ERA5 global reanalysis. *Q. J. R. Meteorol. Soc.* **2020**, *146* (730), 1999−2049.
(53) Zhou, Z.-H.; Feng, J. J. A. Deep Forest. *Nat. Sci. Rev.* **2019**, *6* (1), 74−86.
(54) Wei, J.; Liu, S.; Li, Z.; Liu, C.; Qin, K.; Liu, X.; Pinker, R. T.; Dickerson, R. R.; Lin, J.; Boersma, K. F.; Sun, L.; Li, R.; Xue, W.; Cui, Y.; Zhang, C.; Wang, J. Ground-Level NO_2 Surveillance from Space Across China for High Resolution Using Interpretable Spatiotemporally Weighted Artificial Intelligence. *Environ. Sci. Technol.* **2022**, *56* (14), 9988−9998.
(55) Li, T.; Shen, H.; Yuan, Q.; Zhang, X.; Zhang, L. Estimating Ground-Level $PM_{2.5}$ by Fusing Satellite and Station Observations: A Geo-Intelligent Deep Learning Approach. *Geophys. Res. Lett.* **2017**, *44* (23), 11985−11993.
(56) Wei, J.; Huang, W.; Li, Z.; Xue, W.; Peng, Y.; Sun, L.; Cribb, M. Estimating 1-km-resolution $PM_{2.5}$ concentrations across China using the space-time random forest approach. *Remote Sens. Environ.* **2019**, *231*, 111221.
(57) Wei, J.; Li, Z.; Cribb, M.; Huang, W.; Xue, W.; Sun, L.; Guo, J.; Peng, Y.; Li, J.; Lyapustin, A.; Liu, L.; Wu, H.; Song, Y. Improved 1 km resolution $PM_{2.5}$ estimates across China using enhanced space-time extremely randomized trees. *Atmos. Chem. Phys.* **2020**, *20* (6), 3273−3289.
(58) Sun, H.; Shin, Y. M.; Xia, M.; Ke, S.; Wan, M.; Yuan, L.; Guo, Y.; Archibald, A. T. Spatial Resolved Surface Ozone with Urban and Rural Differentiation during 1990−2019: A Space-Time Bayesian Neural Network Downscaler. *Environ. Sci. Technol.* **2022**, *56* (11), 7337−7349.
(59) Zhai, S.; Jacob, D. J.; Wang, X.; Shen, L.; Li, K.; Zhang, Y.; Gui, K.; Zhao, T.; Liao, H. Fine particulate matter ($PM_{2.5}$) trends in China, 2013−2018: separating contributions from anthropogenic emissions and meteorology. *Atmos. Chem. Phys.* **2019**, *19* (16), 11031−11041.
(60) Zheng, B.; Tong, D.; Li, M.; Liu, F.; Hong, C.; Geng, G.; Li, H.; Li, X.; Peng, L.; Qi, J.; Yan, L.; Zhang, Y.; Zhao, H.; Zheng, Y.; He, K.;

https://doi.org/10.1021/acs.est.3c00272
Environ. Sci. Technol. XXXX, XXX, XXX−XXX

Zhang, Q. Trends in China's anthropogenic emissions since 2010 as the consequence of clean air actions. *Atmos. Chem. Phys.* **2018**, *18* (19), 14095−14111.
(61) Wang, Y.; Zhang, Q. Q.; He, K.; Zhang, Q.; Chai, L. Sulfate-nitrate-ammonium aerosols over China: response to 2000−2015 emission changes of sulfur dioxide, nitrogen oxides, and ammonia. *Atmos. Chem. Phys.* **2013**, *13* (5), 2635−2652.
(62) Zhang, L.; Chen, Y.; Zhao, Y.; Henze, D. K.; Zhu, L.; Song, Y.; Paulot, F.; Liu, X.; Pan, Y.; Lin, Y.; Huang, B. Agricultural ammonia emissions in China: reconciling bottom-up and top-down estimates. *Atmos. Chem. Phys.* **2018**, *18* (1), 339−355.
(63) Wang, S.; Su, H.; Chen, C.; Tao, W.; Streets, D. G.; Lu, Z.; Zheng, B.; Carmichael, G. R.; Lelieveld, J.; Pöschl, U.; Cheng, Y. Natural gas shortages during the ″coal-to-gas″ transition in China have caused a large redistribution of air pollution in winter 2017. *Proc. Natl. Acad. Sci. U.S.A* **2020**, *117* (49), 31018−31025.
(64) Guo, J.; Miao, Y.; Zhang, Y.; Liu, H.; Li, Z.; Zhang, W.; He, J.; Lou, M.; Yan, Y.; Bian, L.; Zhai, P. The climatology of planetary boundary layer height in China derived from radiosonde and reanalysis data. *Atmos. Chem. Phys.* **2016**, *16* (20), 13309−13319.
(65) Guo, J.; Zhang, J.; Yang, K.; Liao, H.; Zhang, S.; Huang, K.; Lv, Y.; Shao, J.; Yu, T.; Tong, B.; Li, J.; Su, T.; Yim, S. H. L.; Stoffelen, A.; Zhai, P.; Xu, X. Investigation of near-global daytime boundary layer height using high-resolution radiosondes: first results and comparison with ERA5, MERRA-2, JRA-55, and NCEP-2 reanalyses. *Atmos. Chem. Phys.* **2021**, *21* (22), 17079−17097.
(66) Li, Y. J.; Sun, Y.; Zhang, Q.; Li, X.; Li, M.; Zhou, Z.; Chan, C. K. Real-time chemical characterization of atmospheric particulate matter in China: A review. *Atmos. Environ.* **2017**, *158*, 270−304.
(67) Guo, J.; Su, T.; Chen, D.; Wang, J.; Li, Z.; Lv, Y.; Guo, X.; Liu, H.; Cribb, M.; Zhai, P. Declining Summertime Local-Scale Precipitation Frequency Over China and the United States, 1981−2012: The Disparate Roles of Aerosols. *Geophys. Res. Lett.* **2019**, *46* (22), 13281−13289.
(68) Hong, C.; Zhang, Q.; Zhang, Y.; Davis, S. J.; Tong, D.; Zheng, Y.; Liu, Z.; Guan, D.; He, K.; Schellnhuber, H. J. Impacts of climate change on future air quality and human health in China. *Proc. Natl. Acad. Sci. U.S.A* **2019**, *116* (35), 17193−17200.
(69) Hand, J. L.; Schichtel, B. A.; Pitchford, M.; Malm, W. C.; Frank, N. H. Seasonal composition of remote and urban fine particulate matter in the United States. *J. Geophys. Res.-Atmos.* **2012**, *117* (D5), 1−22.
(70) Pinder, R. W.; Adams, P. J.; Pandis, S. N. Ammonia Emission Controls as a Cost-Effective Strategy for Reducing Atmospheric Particulate Matter in the Eastern United States. *Environ. Sci. Technol.* **2007**, *41* (2), 380−386.
(71) Liu, P.; Ding, J.; Liu, L.; Xu, W.; Liu, X. Estimation of surface ammonia concentrations and emissions in China from the polar-orbiting Infrared Atmospheric Sounding Interferometer and the FY-4A Geostationary Interferometric Infrared Sounder. *Atmos. Chem. Phys.* **2022**, *22* (13), 9099−9110.
(72) Gao, J.; Yang, Y.; Wang, H.; Wang, P.; Li, H.; Li, M.; Ren, L.; Yue, X.; Liao, H. Fast climate responses to emission reductions in aerosol and ozone precursors in China during 2013−2017. *Atmos. Chem. Phys.* **2022**, *22* (11), 7131−7142.
(73) Zhang, Z.; Zhou, Y.; Zhao, N.; Li, H.; Tohniyaz, B.; Mperejekumana, P.; Hong, Q.; Wu, R.; Li, G.; Sultan, M.; Zayan, A. M. I.; Cao, J.; Ahmad, R.; Dong, R. Clean heating during winter season in Northern China: A review. *Renew. Sust. Energy Rev.* **2021**, *149*, 111339.
(74) Shuangchen, M.; Jin, C.; Kunling, J.; Lan, M.; Sijie, Z.; Kai, W. Environmental influence and countermeasures for high humidity flue gas discharging from power plants. *Renew. Sust. Energy Rev.* **2017**, *73*, 225−235.
(75) Li, C.; Hammer, M. S.; Zheng, B.; Cohen, R. C. Accelerated reduction of air pollutants in China, 2017−2020. *Sci. Total Environ.* **2022**, *803*, 150011.
(76) Zhai, S.; Jacob, D. J.; Wang, X.; Liu, Z.; Wen, T.; Shah, V.; Li, K.; Moch, J. M.; Bates, K. H.; Song, S.; Shen, L.; Zhang, Y.; Luo, G.; Yu, F.; Sun, Y.; Wang, L.; Qi, M.; Tao, J.; Gui, K.; Xu, H.; Zhang, Q.; Zhao, T.; Wang, Y.; Lee, H. C.; Choi, H.; Liao, H. Control of particulate nitrate air pollution in China. *Nat. Geosci.* **2021**, *14* (6), 389−395.
(77) Liu, S.; Geng, G.; Xiao, Q.; Zheng, Y.; Liu, X.; Cheng, J.; Zhang, Q. Tracking Daily Concentrations of $PM_{2.5}$ Chemical Composition in China since 2000. *Environ. Sci. Technol.* **2022**, *56* (22), 16517−16527.
(78) Wang, H.; Wang, H.; Lu, X.; Lu, K.; Zhang, L.; Tham, Y. J.; Shi, Z.; Aikin, K.; Fan, S.; Brown, S. S.; Zhang, Y. Increased night-time oxidation over China despite widespread decrease across the globe. *Nat. Geosci.* **2023**, *16*, 217−223.
(79) Wei, J.; Li, Z.; Xue, W.; Sun, L.; Fan, T.; Liu, L.; Su, T.; Cribb, M. The ChinaHighPM_{10} dataset: generation, validation, and spatiotemporal variations from 2015 to 2019 across China. *Environ. Int.* **2021**, *146*, 106290.
(80) Zhai, S.; Jacob, D. J.; Pendergrass, D. C.; Colombi, N. K.; Shah, V.; Yang, L. H.; Zhang, Q.; Wang, S.; Kim, H.; Sun, Y.; Choi, J. S.; Park, J. S.; Luo, G.; Yu, F.; Woo, J. H.; Kim, Y.; Dibb, J. E.; Lee, T.; Han, J. S.; Anderson, B. E.; Li, K.; Liao, H. Coarse particulate matter air quality in East Asia: implications for fine particulate nitrate. *Atmos. Chem. Phys.* **2023**, *23*, 4271−4281.
(81) Zhang, Q.; Zheng, Y.; Tong, D.; Shao, M.; Wang, S.; Zhang, Y.; Xu, X.; Wang, J.; He, H.; Liu, W.; Ding, Y.; Lei, Y.; Li, J.; Wang, Z.; Zhang, X.; Wang, Y.; Cheng, J.; Liu, Y.; Shi, Q.; Yan, L.; Geng, G.; Hong, C.; Li, M.; Liu, F.; Zheng, B.; Cao, J.; Ding, A.; Gao, J.; Fu, Q.; Huo, J.; Liu, B.; Liu, Z.; Yang, F.; He, K.; Hao, J. Drivers of improved $PM_{2.5}$ air quality in China from 2013 to 2017. *Proc. Natl. Acad. Sci. U.S.A* **2019**, *116* (49), 24463−24469.
(82) Li, C.; Marufu, L. T.; Dickerson, R. R.; Li, Z.; Wen, T.; Wang, Y.; Wang, P.; Chen, H.; Stehr, J. W. In situ measurements of trace gases and aerosol optical properties at a rural site in northern China during East Asian Study of Tropospheric Aerosols: An International Regional Experiment 2005. *J. Geophys. Res.-Atmos.* **2007**, *112* (D22), 1−16.
(83) Feng, T.; Du, H.; Coffman, D. M.; Qu, A.; Dong, Z. Clean heating and heating poverty: A perspective based on cost-benefit analysis. *Energy Policy* **2021**, *152*, 112205.
(84) Lee, E. J.; Kim, M. J.; Lee, J.-S. Policy Implications of the Clean Heating Transition: A Case Study of Shanxi. *Energies* **2021**, *14* (24), 8431.
(85) Chen, H.; Chen, W. Potential impact of shifting coal to gas and electricity for building sectors in 28 major northern cities of China. *Appl. Energy* **2019**, *236*, 1049−1061.
(86) Wu, J.; Bei, N.; Wang, Y.; Li, X.; Liu, S.; Liu, L.; Wang, R.; Yu, J.; Le, T.; Zuo, M.; Shen, Z.; Cao, J.; Tie, X.; Li, G. Insights into particulate matter pollution in the North China Plain during wintertime: local contribution or regional transport? *Atmos. Chem. Phys.* **2021**, *21* (3), 2229−2249.
(87) Fu, X.; Wang, T.; Gao, J.; Wang, P.; Liu, Y.; Wang, S.; Zhao, B.; Xue, L. Persistent Heavy Winter Nitrate Pollution Driven by Increased Photochemical Oxidants in Northern China. *Environ. Sci. Technol.* **2020**, *54* (7), 3881−3889.
(88) Wang, T.; Liu, M.; Liu, M.; Song, Y.; Xu, Z.; Shang, F.; Huang, X.; Liao, W.; Wang, W.; Ge, M.; Cao, J.; Hu, J.; Tang, G.; Pan, Y.; Hu, M.; Zhu, T. Sulfate Formation Apportionment during Winter Haze Events in North China. *Environ. Sci. Technol.* **2022**, *56* (12), 7771−7778.
(89) Zheng, B.; Zhang, Q.; Geng, G.; Chen, C.; Shi, Q.; Cui, M.; Lei, Y.; He, K. Changes in China's anthropogenic emissions and air quality during the COVID-19 pandemic in 2020. *Earth Syst. Sci. Data* **2021**, *13* (6), 2895−2907.
(90) Yang, Y.; Ren, L.; Wu, M.; Wang, H.; Song, F.; Leung, L. R.; Hao, X.; Li, J.; Chen, L.; Li, H.; Zeng, L.; Zhou, Y.; Wang, P.; Liao, H.; Wang, J.; Zhou, Z.-Q. Abrupt emissions reductions during COVID-19 contributed to record summer rainfall in China. *Nat. Commun.* **2022**, *13* (1), 959.

https://doi.org/10.1021/acs.est.3c00272
Environ. Sci. Technol. XXXX, XXX, XXX−XXX

(91) Zhao, X.; Wang, G.; Wang, S.; Zhao, N.; Zhang, M.; Yue, W. Impacts of COVID-19 on air quality in mid-eastern China: An insight into meteorology and emissions. *Atmos. Environ.* **2021**, *266*, 118750.
(92) Xian, T.; Li, Z.; Wei, J. Changes in Air Pollution Following the COVID-19 Epidemic in Northern China: The Role of Meteorology. *Front. Environ. Sci.* **2021**, *9*, 654651.
(93) Hammer, M. S.; van Donkelaar, A.; Martin, R. V.; McDuffie, E. E.; Lyapustin, A.; Sayer, A. M.; Hsu, N. C.; Levy, R. C.; Garay, M. J.; Kalashnikova, O. V.; Kahn, R. A. Effects of COVID-19 lockdowns on fine particulate matter concentrations. *Sci. Adv.* **2021**, *7* (26), No. eabg7670.
(94) Su, T.; Li, Z.; Zheng, Y.; Luan, Q.; Guo, J. Abnormally Shallow Boundary Layer Associated With Severe Air Pollution During the COVID-19 Lockdown in China. *Geophys. Res. Lett.* **2020**, *47* (20), No. e2020GL090041.
(95) Li, K.; Jacob, D. J.; Liao, H.; Qiu, Y.; Shen, L.; Zhai, S.; Bates, K. H.; Sulprizio, M. P.; Song, S.; Lu, X.; Zhang, Q.; Zheng, B.; Zhang, Y.; Zhang, J.; Lee, H. C.; Kuk, S. K. Ozone pollution in the North China Plain spreading into the late-winter haze season. *Proc. Natl. Acad. Sci. U.S.A* **2021**, *118* (10), No. e2015797118.
(96) Shi, X.; Brasseur, G. P. The Response in Air Quality to the Reduction of Chinese Economic Activities During the COVID-19 Outbreak. *Geophys. Res. Lett.* **2020**, *47* (11), No. e2020GL088070.
(97) Huang, X.; Ding, A.; Gao, J.; Zheng, B.; Zhou, D.; Qi, X.; Tang, R.; Wang, J.; Ren, C.; Nie, W.; Chi, X.; Xu, Z.; Chen, L.; Li, Y.; Che, F.; Pang, N.; Wang, H.; Tong, D.; Qin, W.; Cheng, W.; Liu, W.; Fu, Q.; Liu, B.; Chai, F.; Davis, S. J.; Zhang, Q.; He, K. Enhanced secondary pollution offset reduction of primary emissions during COVID-19 lockdown in China. *Nat. Sci. Rev.* **2021**, *8* (2), nwaa137.

NOTE ADDED AFTER ASAP PUBLICATION

This paper was published ASAP on April 28, 2023, with an error in the TOC graphic. The corrected version was reposted on May 2, 2023.

https://doi.org/10.1021/acs.est.3c00272
Environ. Sci. Technol. XXXX, XXX, XXX−XXX